



Fast one-step preparation of porous carbon with hierarchical oxygen-enriched structure from waste lignin for chloramphenicol removal

Aixia Chen^{1,2} · Jiaju Pang^{1,2} · Xiao Wei^{1,2} · Bei Chen³ · Yaping Xie^{1,2}

Received: 29 October 2020 / Accepted: 20 January 2021 / Published online: 28 January 2021
© The Author(s), under exclusive licence to Springer-Verlag GmbH, DE part of Springer Nature 2021

Abstract

This work explored the use of porous carbon (PC) materials converted from waste lignin as raw materials for the removal of chloramphenicol (CAP) in water. The PC with controllable pores was prepared through a facile, cost-effective one-step method. The physical and chemical properties of the material were characterized by BET, SEM, FT-IR, and XRD, and the best conditions for preparation were selected based on the results of adsorption experiments. The PC, which was prepared at reaction temperature of 800 °C and the K₂CO₃/sodium lignosulfonate mass ratio of 4, namely PC-800-4, had a high specific surface area (1305.5 m² g⁻¹) and pore volume (0.758 cm³ g⁻¹). At a lower initial concentration of CAP (C₀ = 120 mg L⁻¹), the maximum adsorption capacity of this adsorbent was 534.0 mg g⁻¹ at 303 K. In addition, PC-800-4 maintained good adsorption performance in a wide pH range and strongly resisted the interference of ions and humic acid. The results showed that the adsorption removal CAP was based on physical adsorption and chemical adsorption as a process supplement. The advantages of wide sources, high efficiency and speed, wide application, and rich oxygen-containing functional groups made the adsorbent have great application potential for removal chloramphenicol from water.

Keywords Adsorption · Porous carbons · Sodium lignosulfonate · One-step method · Chloramphenicol

Introduction

In recent decades, reports of antibiotics detected in water have become more frequent (Wei et al. 2019). Antibiotics are

considered as new pollutants due to their trace, bioaccumulative, hardly degradable, and persistent properties (Wang and Chu 2016). Most of the antibiotics administered into the living organism cannot be completely absorbed

Aixia Chen and Jiaju Pang contributed equally to this work.

Highlights

Porous carbon can be quickly prepared by one-step method.
PC-800-4 had a high specific surface area (1305.5 m² g⁻¹) and pore volume (0.758 cm³ g⁻¹).
PC-800-4 had ultrahigh adsorption capacity of 534.0 mg g⁻¹ for chloramphenicol at 303 k.
The strong anti-interference ability and high adsorption capacity made PC-800-4 have huge application potential.

Responsible Editor: Tito Roberto Cadaval Jr

✉ Aixia Chen
aixiach@chd.edu.cn

✉ Xiao Wei
chdwx@chd.edu.cn

² Key Laboratory of Subsurface Hydrology and Ecological Effects in Arid Region, Ministry of Education, Chang'an University, Xi'an 710054, China

³ Haiwei Environmental Technology Company, Chang'an University, Xi'an 710054, China

¹ School of Water and Environment, Chang'an University, Xi'an 710054, China

(Carvalho and Santos 2016; Wang et al. 2020), causing a large quantity of antibiotics to be discharged into environment. Chloramphenicol is a broad-spectrum antibiotic that is widely used in human and veterinary medicines because of its low cost and inhibitory effect on a variety of bacterial infections, including gram-negative and typhoid bacteria. It is a stronger bactericidal agent than penicillin and tetracycline (Liu et al. 2017a). CAP has many side effects on the human body, including gray baby syndrome (Mauer et al. 1980), aplastic anemia (Clesham et al. 2019), and bone marrow suppression (Jimenez et al. 1990). Therefore, many countries including China (Liu et al. 2017b), the USA (George and Hall 2002), and Japan (Kikuchi et al. 2017) strictly prohibit the use of CAP for livestock breeding. However, CAP is still commonly used in many developing countries because it is inexpensive and effective. In order to solve the problem of antibiotic pollution, especially in water, many treatment technologies have been developed such as membrane separation (Srinivasa Raghavan et al. 2018), redox (Ye et al. 2020), adsorption (LÜ et al. 2012), and catalysis (Lu et al. 2019). In a variety of technologies, adsorption is most preferable and widely used because of its low cost, high efficiency, and simple operation (Li et al. 2019).

Porous carbon materials were widely used for pollutant removal due to their large specific surface area, rich porosity, and high corrosion resistance (Awual and Hasan. 2015; Awual. 2017a). Biomass materials have attracted widespread attention due to their abundance, availability, and environmental friendliness (Chen et al. 2021; Liu et al. 2019). Till date, there have been numerous reports on the usage of different biomass materials as carbon sources to develop carbon materials for specific uses. For instance, bovine bones are abundant in inorganic hydroxyapatite and organic collagen, which can be carbonized by self-template carbonization and then in-situ alkali-activation to produce porous carbon materials (Dai et al. 2018a). Facts have proved that the prepared material has significant adsorption capacity for sulfamethazine and CAP antibiotics. Furthermore, biomass, including shiitake mushroom (Cheng et al. 2015), coconut shell (Dissanayake Herath et al. 2019), and auricularia (Xie et al. 2019a), have also been used as raw materials for making porous carbon. Optically, conjugated porous materials have high selectivity and sensitivity to pollutants (Awual. 2019a; 2017b; 2016a), while porous carbon materials have the advantages of rapid and high adsorption capacity.

Studies have found that oxygen-containing functional groups such as carboxyl, carbonyl, phenols, lactones, and quinones could greatly affect the unique adsorption performance of activated carbon to pollutants (Bhatnagar et al. 2013). They can combine heavy metal ions and organic small molecule pollutants through chelation, coordination, and hydrogen bonding (Zhang et al. 2015). Agricultural by-products not only have functional groups such as carboxyl and hydroxyl groups, but also have the characteristics of loose and porous

structure, which are good precursors for adsorption materials (Dai et al. 2018b; Zhou et al. 2015). Lignin is a renewable carbon source and is the second largest biopolymer on earth after cellulose. Despite the potential for large-scale use of lignin, it is worth noting as at today that humans use only 3% of lignin. Sodium lignosulfonate (SLS), as a by-product of lignin used in the paper industry, generates approximately 70 million tons per year (Liu et al. 2015). Compared with lignin, SLS still contains more oxygen-containing functional groups, such as α -O-4' and β -O-4' linkages (Abukhadra et al. 2019; Galkin and Samec 2016), which can significantly improve water solubility and expand the scope of application. Hence, SLS may be the most promising carbon raw material. Literature evidence indicates that lignin-based porous carbon materials have been successfully used to remove heavy metals and dyes from water (Wu et al. 2020; Zhang et al. 2019). Therefore, it makes great sense to use SLS for the preparation of porous carbons to remove CAP. As far as we know, there have been no such reports before.

Based on the International Union of Pure and Applied Chemistry (IUPAC) specifications, pores have been divided into three types based on their diameter: micropores (< 2 nm), mesopores (2–50 nm), and macropores (> 50 nm). Research has shown that micropores and small mesopores can expand the specific surface area of porous carbon, while large mesopores and macropores are conducive for the transport of target molecules (Yang et al. 2019; Lv et al. 2016; Awual and Hasan. 2014). Therefore, in order to improve the ability of porous carbon to absorb pollutants, it is necessary to reconfigure its pore structure. Carbon raw materials can be converted into activated carbon by physical or chemical activation. Compared with the former, carbon produced by chemical activation method has better pore structure and specific surface area (Gao et al. 2013). However, common chemical activation methods for the preparation of porous carbon require the use of templates. The process involves a series of time-consuming template carbonization, template removal, and subsequent activation, which will greatly increase production costs (Xie et al. 2019b). For non-template method, Oginni et al. (Oginni et al. 2019) showed that the one-step method produced porous carbon with larger specific areas, total pore volumes, and average pore diameters than the two-step method, which were carbon-carbonized and then activated. More importantly, the porous carbon prepared by one-step method exhibited higher adsorption capacity.

In this work, a simple method was proposed for making layered, porous carbons (PCs) by using SLS as carbon precursor. By adjusting temperature and the mass ratio of activator K_2CO_3 to SLS, porous carbons with different pore structures were prepared through the one-step method. With CAP as the target pollutant, the removal mechanism and applicability of PCs were explored. This study showcased several advantages derivable from the fabrication of lignin porous carbon by the

one-step method. These include (1) the one-step method greatly simplifies the manufacturing process of porous carbon materials and reduces the preparation cost and time and (2) abundance and availability of economical carbon raw materials make PCs promising as a large-scale practical applications adsorbent. With these advantages, PCs can be used as a viable, economical, and efficient adsorbent for the removal of antibiotics in the environment.

Materials and methods

Materials and reagents

CAP ($C_{11}H_{12}C_{12}N_2O_5$, 98%), SLS, and potassium carbonate (K_2CO_3 , 99%) were purchased from Aladdin Industrial Corporation (Shanghai, China). All chemicals were of analytical grade, without any further purifications.

Preparation of PCs

PCs were prepared as follows: 4.0 g of SLS with different masses of K_2CO_3 (0 g, 4.0 g, 8.0 g, 12.0 g, 16.0 g) were ground, mixed, and placed in a tube furnace. Under the protection of N_2 flow, the temperature was raised from room temperature to 750 °C, 800 °C, 850 °C at the rate of 5 °C min^{-1} and maintained for 2 h. The reaction mixture was then cooled to room temperature. Afterwards, the black powder was washed with dilute hydrochloric acid and hot deionized water to remove inorganic impurities such as potassium compounds. The resulting powder was purified by washing with water several times and subsequently dried at 105 °C. The product was expressed as PC-*T*-*x*, where *T* and *x* represent activation temperature and mass ratio of K_2CO_3 /SLS, respectively.

Characterization methods

The topographic characteristics of the synthesized PCs were determined by scanning electron microscopy (SEM, S-4800, Hitachi, Japan) and X-ray diffraction (XRD, D8 ADVANCE, Bruker AXS, Germany) technique. The Fourier transform infrared spectroscopy (FT-IR) was performed on a Spectrum Two spectrophotometer (PerkinElmer, USA) with KBr pellets. N_2 adsorption-desorption isotherms were determined by ASAP 2020 PLUS (Micromeritics, USA) volumetric instrument at 77 K.

Batch adsorption experiments

To investigate the effect of the mass ratios of K_2CO_3 and SLS on the adsorption properties of the synthesized PCs, 3.0 mg of PC-800-*x* adsorbent was used to adsorb 20 mL CAP solution

(100 mg L^{-1}) for 12 h in water. After filtration, the CAP concentration in the supernatant was calculated from the absorbance readings taken at 278 nm in a UV spectrophotometer. Subsequently, in order to study the effect of pyrolysis temperature on adsorption, the above experiment was repeated using PC-750-4 and PC-850-4. The adsorption and BET results showed that PC-800-4 had the second highest microporosity and adsorption capacity for CAP. In order to obtain accurate data, all experiments were performed three times, and the average data was obtained for the next analysis.

In another experiment, the effects of pH (2–12), initial CAP concentration, metal ion concentration, humic acid, and temperature on the adsorption of CAP by PC-800-4 were investigated. The pH affects the form of ions in the solution (Awual 2019b; 2016b). We first explored the effect of pH on adsorption and determined the best adsorption conditions for subsequent experiments. For the adsorption isotherm experiment, 3.0 mg of PC-800-4 was added to the CAP aqueous solution with different initial concentrations (50, 75, 100, 120, 135 mg L^{-1}). After equilibration in a 303 K water bath for 12 h, the adsorption equilibrium was reached. The adsorbent PC-800-4 was separated by filtration, and the concentration of non-adsorbed CAP molecules was measured at 278 nm using an ultraviolet-visible spectrophotometer. The equilibrium adsorption capacity for CAP was calculated by the following formula.

$$Q_e = (C_0 - C_e) \times \frac{V}{M} \quad (1)$$

where C_0 and C_e (mg L^{-1}) represent the initial and adsorption equilibrium concentrations of the CAP solution, respectively; V (mL) is the solution volume and M (mg) is the weight of adsorbent.

The influence of solution pH on adsorption was investigated. The CAP solution (120 mg L^{-1}) was adjusted to 2.0–12 with 0.1 M dilute HCl and NaOH solution. At 303 K, 3.0 mg of PC-800-4 was put into 20 mL of CAP solution of different pHs for adsorption. In addition, the effects of 0.1 M common metal ions (K^+ , Na^+ , Ca^{2+} , Mg^{2+} , Al^{3+}) and different concentrations (10, 30, 50, 70 mg L^{-1}) of humic acid on the adsorption of CAP solution (100 mg L^{-1}) were also studied.

Adsorption kinetics was used to study the effect of contact time on the amount of adsorption (Awual 2019). In the study, 3.0 mg of PC-800-4 and 20 mL of CAP aqueous solution ($C_0 = 120$ mg L^{-1}) were added to the centrifuge tube. At 303 K, CAP in the supernatant was measured in a regular time (5, 10, 15, 30, 45, 60, 90, 120, 180, 240, 300, and 420 min). In addition, the above experiment was repeated using PC-750-4 and PC-850-4 for comparison. At time t (min), the adsorption capacity Q_t (mg g^{-1}) is calculated as follows.

$$Q_t = (C_0 - C_t) \times \frac{V}{M} \quad (2)$$

where Q_t (mg g^{-1}) is the quantity of CAP absorbed on the adsorbent at the setting time t .

Adsorption isotherms

Adsorption isotherms are useful for understanding the interaction between PC-800-4 and CAP. Langmuir, Freundlich, and Temkin adsorption isotherm models were used to fit the data in this experiment. The nonlinear expressions are as follows.

$$\text{Langmuir : } Q_e = \frac{Q_m \times K_L \times C_e}{1 + K_L \times C_e} \tag{3}$$

$$\text{Freundlich : } Q_e = K_F \times C_e^{1/n} \tag{4}$$

$$\text{Temkin : } Q_e = b \ln K_t + b \ln C_e \tag{5}$$

where Q_m (mg g^{-1}) is the maximum adsorption for CAP per unit mass of carbon; K_L (L mg^{-1}), K_F (mg g^{-1}) ($(\text{L mg}^{-1})^{1/n}$) are Langmuir (3) and Freundlich (4) constant, respectively; $1/n$ is a measure of the adsorption intensity; b related to the adsorption heat is the Temkin (5) constant, and K_t is the equilibrium-binding constant.

Adsorption kinetics

To figure out the adsorption mechanism of CAP, pseudo-first-order, pseudo-second-order, and intra-particle diffusion kinetic models were used to fit and analyze the experimentally obtained kinetic data. The nonlinear equations for the three models are as follows.

$$\text{Pseudo-first-order model : } Q_t = Q_e \times (1 - e^{-k_1 t}) \tag{6}$$

$$\text{Pseudo-second-order model : } Q_t = Q_e \times \left(1 - \frac{1}{1 + Q_e \times k_2 t} \right) \tag{7}$$

$$\text{Intra-particle diffusion kinetic model : } Q_t = K_{pi} t^{1/2} + C_i \tag{8}$$

where Q_e and Q_t (mg g^{-1}) are the quantity of CAP absorbed on the PC-800-4 at equilibrium and setting time t ; K_1 (min^{-1}), K_2 ($\text{g mg}^{-1} \text{min}^{-1}$), and K_{pi} ($\text{mg (g min}^{1/2})^{-1}$) are the pseudo-first-order, pseudo-second-order, and intra-particle diffusion rate constant; C_i is a constant of Eq. (8).

Adsorption thermodynamics

Changes in thermodynamic parameters, Gibbs free energy change (ΔG), enthalpy change (ΔH), and entropy change (ΔS) during the adsorption process were monitored in order to understand the adsorption behavior and determine its mechanism. Quantitative changes were measured using the following equations.

$$\Delta G = \Delta H - T\Delta S \tag{9}$$

$$\Delta G = -RT \times \ln K_d \tag{10}$$

$$K_d = \frac{(C_0 - C_e)}{C_e} \times \frac{V}{m} \tag{11}$$

where, ΔG is the adsorption free energy change, kJ mol^{-1} ; ΔH is the adsorption enthalpy change, kJ mol^{-1} ; ΔS is the adsorption entropy change, $\text{kJ mol}^{-1} \text{K}^{-1}$; R is the ideal gas constant ($8.314 \text{ J (mol K)}^{-1}$); T is the thermodynamics temperature (K); and K_d is the equilibrium distribution coefficient of adsorption.

Mean free adsorption energy

The Dubinin-Radushkevitch (D-R) adsorption isotherm model has been widely used to measure adsorption, especially for microporous carbon. The nonlinear form of the D-R isotherm equation is as follows.

$$\ln Q_e = Q_{\max} - \ln \beta \varepsilon^2 \tag{12}$$

$$\varepsilon = RT \times \ln \left(1 + \frac{1}{C_e} \right) \tag{13}$$

$$E = \frac{1}{\sqrt{2\beta}} \tag{14}$$

where Q_{\max} is the amount of adsorption in the saturated state; β is the correlation constant with the average free energy of adsorption. ε is Polanyi potential energy, J mol^{-1} . E is the mean free energy of adsorbate unit molecule from the solution to the surface of the adsorbent.

E is an important index to distinguish between physical adsorption and chemical adsorption. If the value of E is less than 8 kJ mol^{-1} , or is between 8 and 16 kJ mol^{-1} or greater than 20 kJ mol^{-1} , it indicates that the adsorption process is physical adsorption, ion exchange chemical adsorption, and chemical adsorption, respectively (Sarkar and Paul 2020).

The average relative error analysis

The average relative error (ARE) (%) is used to evaluate which model is most appropriate to describe the actual data. ARE (%) can be calculated by the following formula.

$$\text{ARE} = \frac{100}{n} \sum_i^n \left| \frac{Q_{i,\text{cal}} - Q_{i,\text{exp}}}{Q_{i,\text{exp}}} \right| \tag{15}$$

where $Q_{i,\text{exp}}$ and $Q_{i,\text{cal}}$ (mg g^{-1}) are the experimental and fitted adsorption quantity, respectively.

Results and discussion

Material characterization

Figure 1 a–c are the SEM images of PC-800-0, PC-800-2, and PC-800-4, respectively. It was observed that as the mass of K_2CO_3 increased, carbon particles became finer and more porous morphologically. This is because K_2CO_3 decomposes into K_2O and CO_2 at any temperature greater than $700\text{ }^\circ\text{C}$, thereby initiating a reaction of K_2O and CO_2 with carbon (C) to form potassium (K) vapor and carbon monoxide (CO), respectively. More porous carbons are formed when K vapor is inserted into the carbon matrix. The reaction sequence of these processes can be depicted as follows (Saygılı and Saygılı 2019).

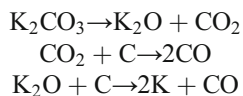


Figure 1 d is a high-resolution SEM image of PC-800-4. It was evident that a large number of pore structures were evenly distributed on the surface of the carbon particles, which served

as transportation channels and provided a large surface area for adsorption of target pollutants in wastewater. The above results showed that PC-800-4 was a porous carbon with excellent pores.

The FT-IR spectra of SLS, PC-800-0 and PC-800-4 are shown in Fig. 2. The broad peak at 3401 cm^{-1} is caused by the stretching vibration of the hydroxyl group. After SLS was carbonized and activated, the products PC-800-0 and PC-800-4 showed gradually weaker peaks for the hydroxyl stretching vibration. In the SLS and PC-800-0 spectra, the absorption peaks at 2938 and 2843 cm^{-1} correspond to the C–H stretching vibration. The characteristic peaks of the aromatic structure skeleton vibration in the SLS molecule are located at 1599 , 1517 , 1463 , 1427 , and 1328 cm^{-1} ; and the stretching vibration peaks of C–O in carboxylic acids, alcohols, phenols, and esters are located at 1219 and 1037 cm^{-1} (Zhang et al. 2011). In addition, the absorption peak of $\beta\text{-O-4'}$ ether bond is located at 1140 cm^{-1} . Compared with the infrared spectrum of SLS, most of the characteristic peaks in the spectrum of the carbonized PC-800-0 showed greatly reduced intensity or disappeared. In the spectrum of PC-800-4, the

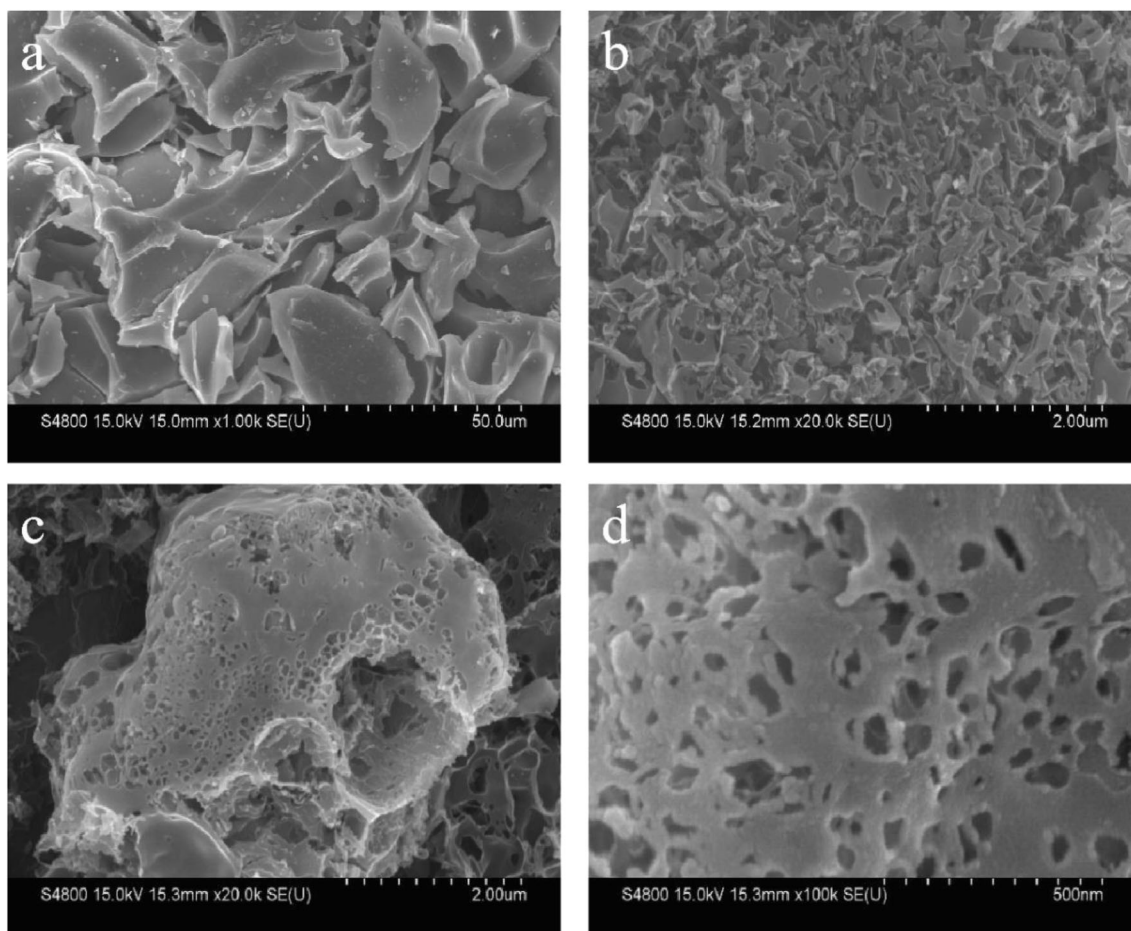


Fig. 1 SEM images of synthesized porous carbons. **a** PC-800-0. **b** PC-800-2. **c, d** PC-800-4

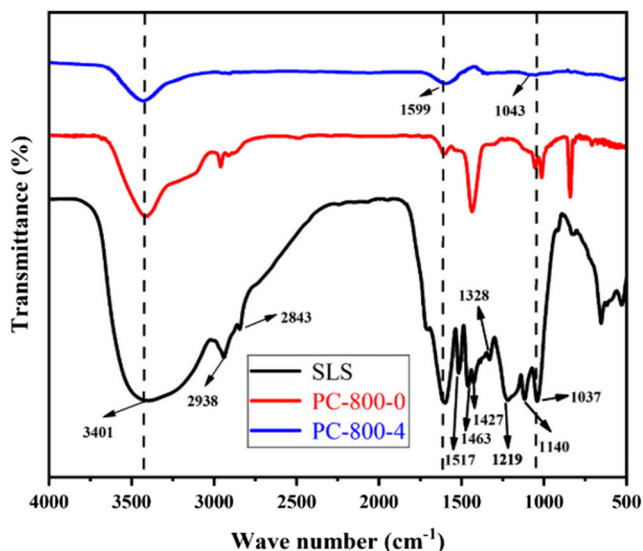


Fig. 2 FT-IR spectra of SLS, PC-800-0, and PC-800-4

absorption peaks at 1599 and 1043 cm^{-1} confirmed the existence of C=O and sulfonic acid groups, respectively (Xie et al. 2019a). The results showed that the carbonization and activation steps affected the surface groups and chemical properties of the product.

In order to explore the crystalline/amorphous properties of PC-800-4, XRD characterization was performed over the 2θ range of $10\text{--}80^\circ$. As shown in Fig. 3, the (002) peak of hexagonal graphitic carbon appeared at $2\theta = 29^\circ$ (Yang et al. 2020a). Compared with PC-800-0, the (002) peak of PC-800-4 was higher and narrower, indicating that the latter had a higher degree of graphitization. The peak at 43° corresponds to the (100) plane of single-layer

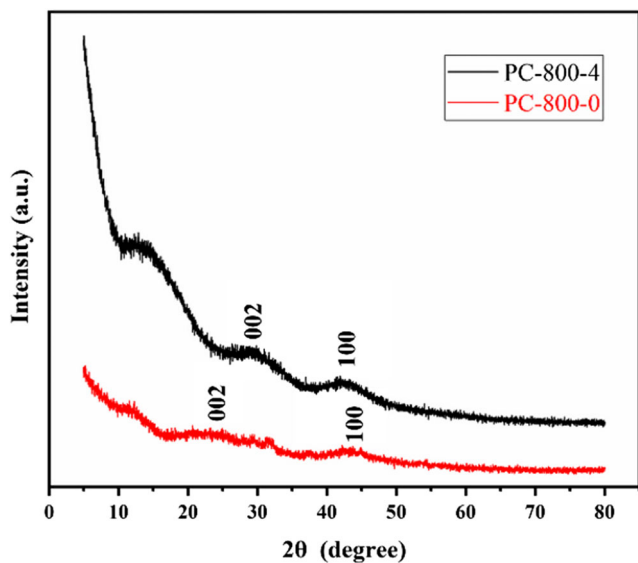


Fig. 3 XRD patterns of PC-800-0 and PC-800-4

graphene honeycomb lattice (Tian et al. 2017), indicating the existence of short-range ordered and parallel-stacked graphite crystallites. During the activation process, SLS (carbon source) was converted into a mixture of defective carbon and graphitic carbon. Defective carbon and graphitic carbon help to enrich pores and promote crystal structure, respectively.

Figure 4 a shows the N_2 adsorption-desorption isotherm of PC- T - x . According to the IUPAC classification, all isotherm curves are of type I, indicating that PCs have microporous structures. Table 1 lists the structural parameters of PC- T - x . The results showed that increasing the temperature or the ratio of $\text{K}_2\text{CO}_3/\text{SLS}$ was beneficial to improve specific surface area and pore volume. At the same temperature, when x increased from 0 to 4, the specific surface area increased from 581.8 to $1305.5 \text{ m}^2 \text{ g}^{-1}$, and the pore volume increased from 0.328 to $0.758 \text{ cm}^3 \text{ g}^{-1}$. When the weight ratio was 4, the specific surface areas of PC-750-4 and PC-850-4 were $1044.1 \text{ m}^2 \text{ g}^{-1}$ and $1522.6 \text{ m}^2 \text{ g}^{-1}$, respectively. It was worth noting that PC-850-4 showed the highest pore volume ($0.864 \text{ cm}^3 \text{ g}^{-1}$). This may be because more potassium vapor and carbon dioxide were released at higher temperatures during the activation process. However, the microporosity of PC-850-4 was lower than that of PC-800-4 and PC-750-4, which can be attributed to the destruction of pore structure caused by high activation temperature. It can be seen from Fig. 4b that the pore diameters of the five porous carbons are mainly less than 2.5 nm . Thus, the porous carbons with abundant mesopores and micropores would have potential applications for CAP adsorption.

Effect of activation parameters

Figure 5 shows the adsorption capacity of PC- T - x for CAP ($C_0 = 100 \text{ mg L}^{-1}$) at 303 K . It can be seen that at the same activation temperature (800°C), increasing the amount of K_2CO_3 significantly improved the adsorption capacity of porous carbon materials. For example, the adsorption capacities of PC-800-1, PC-800-2, PC-800-3, and PC-800-4 were 200.1 , 392.8 , 409.6 , and 511.9 mg g^{-1} , respectively. Similarly, the adsorption capacity increased as the activation temperature was increased under the same experimental conditions. For example, at the $\text{K}_2\text{CO}_3/\text{SLS}$ mass ratio of 4, the adsorption capacity of porous carbon materials for CAP increased from 444.5 to 589.6 mg g^{-1} as the activation temperature rose from 750 to 850°C . The adsorption capacity was consistent with the BET results, indicating that the highly porous structure was the key to improved adsorption. In short, the activation conditions had a significant influence on the adsorption capacity of the adsorbent by affecting

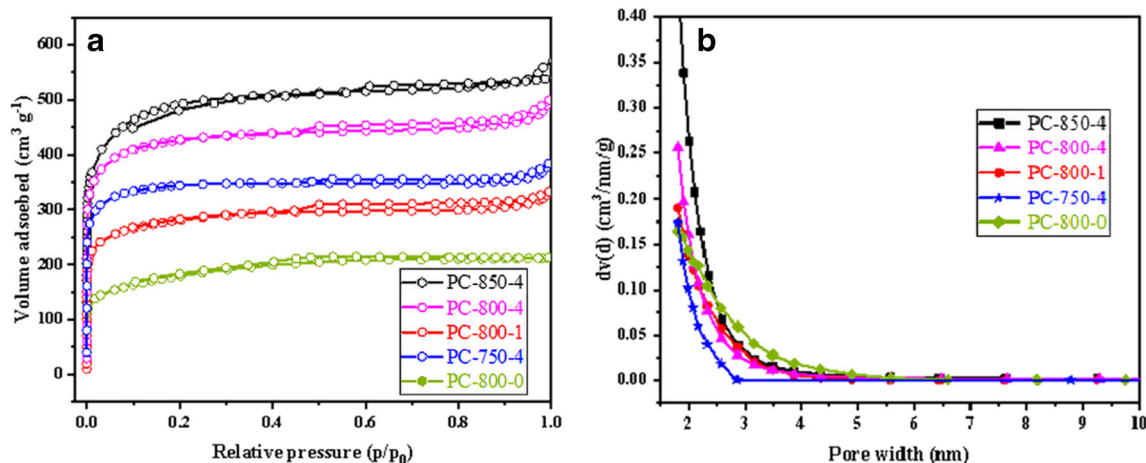


Fig. 4 **a** N_2 adsorption-desorption isotherms and **b** pore size distribution of PC-*T*-*x*

its specific surface area, pore volume, surface chemical properties, and product pore structure.

Effects of solution pH, ion strength, and humic acid

The influence of pH on CAP adsorption was studied under the condition of $C_0 = 120 \text{ mg L}^{-1}$. As shown in Fig. 6a, pH has a slight effect on the adsorption of PC-800-4. The adsorption capacity increased slightly at pH 2–4, but decreased slightly in the range of pH 6–9, indicating that the electrostatic interaction between PC-800-4 and CAP affected the adsorption capacity of the adsorbent. This implied that PC-800-4 could maintain its high-efficiency adsorption capacity for CAP in acid-base environment, which expanded the practical application

range of the adsorbent. Under the natural pH (4.86), the adsorption capacity did not change much, so the original pH was selected as the best condition for subsequent experiments.

Most often, sewage is a mixed solution containing metal ions and humic acid. Therefore, we also investigated the effects of common metal ions and humic acid concentrations on the adsorption of CAP on PC-800-4. As shown in Fig. 6b, at high concentration of 0.1 M, monovalent metal ions (K^+ , Na^+) had little effect on adsorption. However, the adsorption capacity of PC-800-4 was increased by multi-valent metal ions in the order $Al^{3+} > Mg^{2+} > Ca^{2+}$, which was consistent with the order of metal reactivity. This could also have been caused by the strong electrostatic interactions between the PC-800-4 and the multi-valent cations. Figure 6c shows that the

Table 1 Textural properties of PC-800-0 and PC-*T*-*x*

Parameters	PC-800-0	PC-800-1	PC-750-4	PC-800-4	PC-850-4
Specific surface area ($m^2 g^{-1}$)	581.8	879.6	1044.1	1305.5	1522.6
Micropore surface area ($m^2 g^{-1}$)	226.8	551.3	829.3	934.9	987.7
Total surface volume ($cm^3 g^{-1}$)	0.328	0.506	0.586	0.758	0.864
Micropore volume ($cm^3 g^{-1}$)	0.122	0.294	0.438	0.497	0.526
Microporosity (%)	37.01	58.02	75.24	65.6	60.84
Average pore size (nm)	2.26	2.31	2.23	2.32	2.27

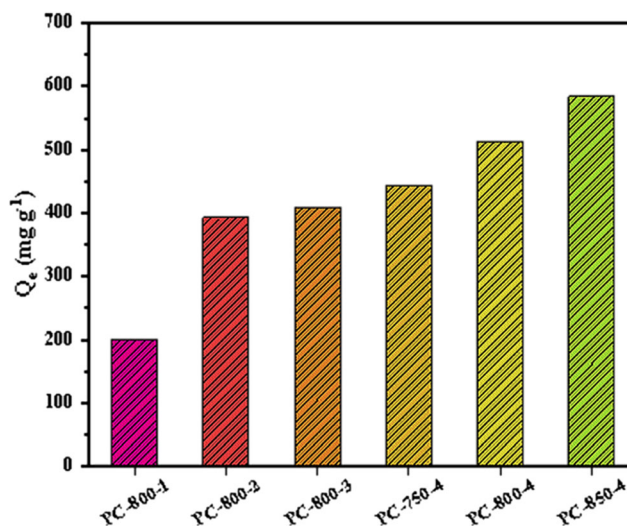


Fig. 5 Comparison of adsorption capacities of PC-*T*-*x* for CAP at 303 K

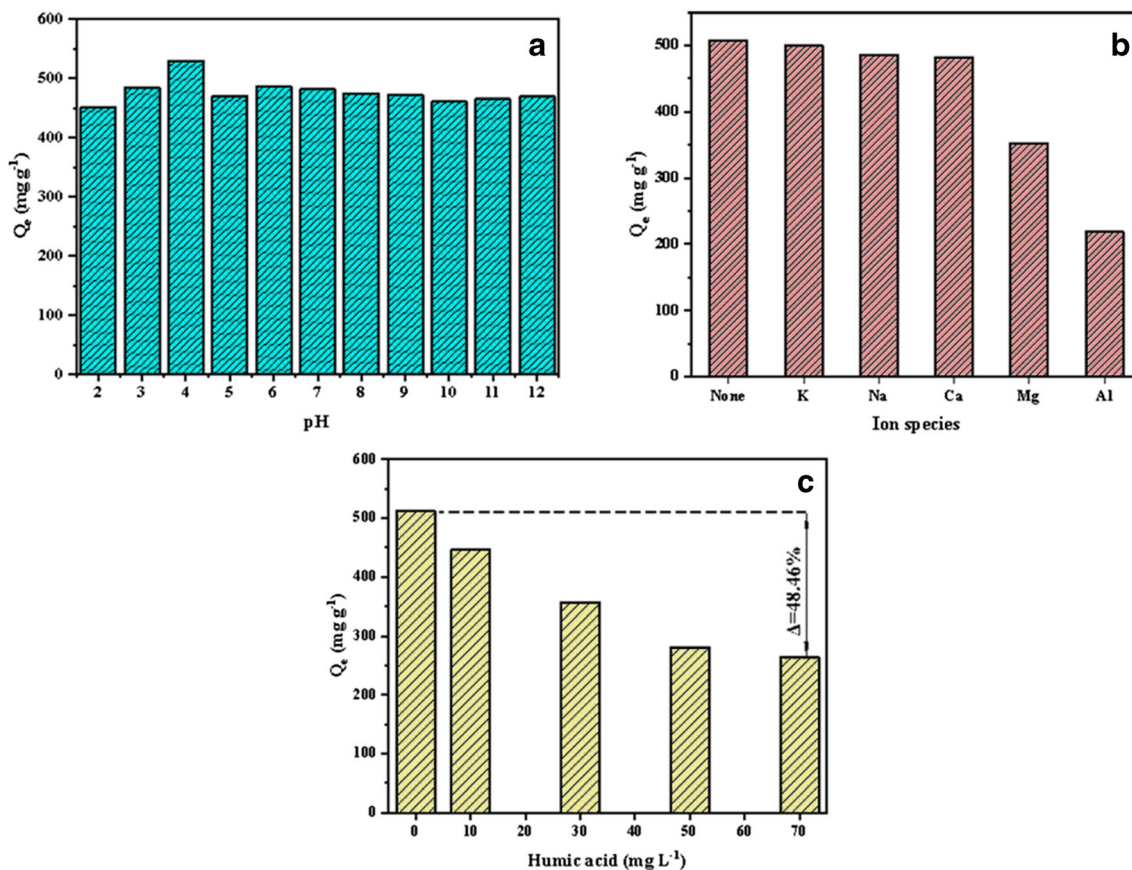


Fig. 6 a Effects of solution pH, b ion species and concentration, c humic acid on CAP adsorption towards PC-800-4 ($T = 303\text{ K}$)

presence of humic acid has a significant effect on the adsorption capacity of PC-800-4 for CAP. This may be caused by the competitive adsorption between humic acid

and CAP molecules in the solution through hydrogen bonding and π - π EDA interactions. It is noteworthy also that under high humic acid conditions (70 mg L^{-1}), the

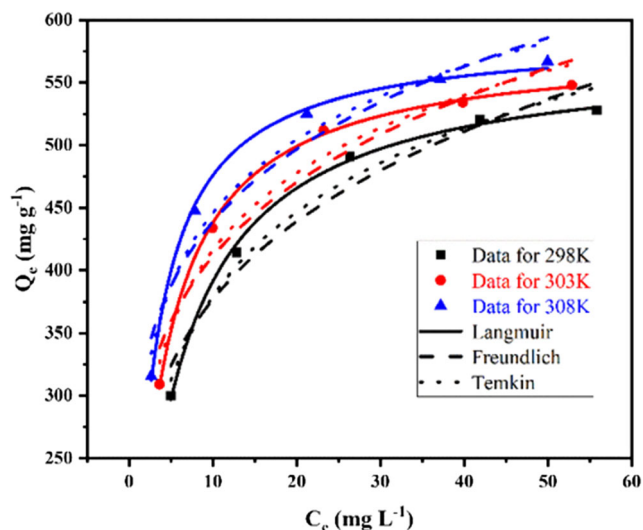


Fig. 7 Adsorption experimental plots and nonlinear fitting curves of CAP adsorption onto PC-850-4

Table 2 Langmuir, Freundlich, and Temkin isotherm model parameters

Model		T (K)		
		298	303	308
Langmuir	Q_m (mg ⁻¹)	574.8	580	587.8
	K_L (L mg ⁻¹)	0.213	0.309	0.425
	R^2	0.9976	0.9992	0.9982
	ARE (%)	0.92	0.63	0.77
Freundlich	K_F (mg g ⁻¹) (L min ⁻¹) ^{1/n}	227.4	263.2	290.4
	1/n	0.22	0.19	0.18
	R^2	0.9786	0.9931	0.9942
	ARE (%)	4.35	4.85	4.82
Temkin	K_T	5.02	10.65	19.43
	R^2	0.975	0.965	0.9687
	ARE (%)	2.82	3.51	3.46

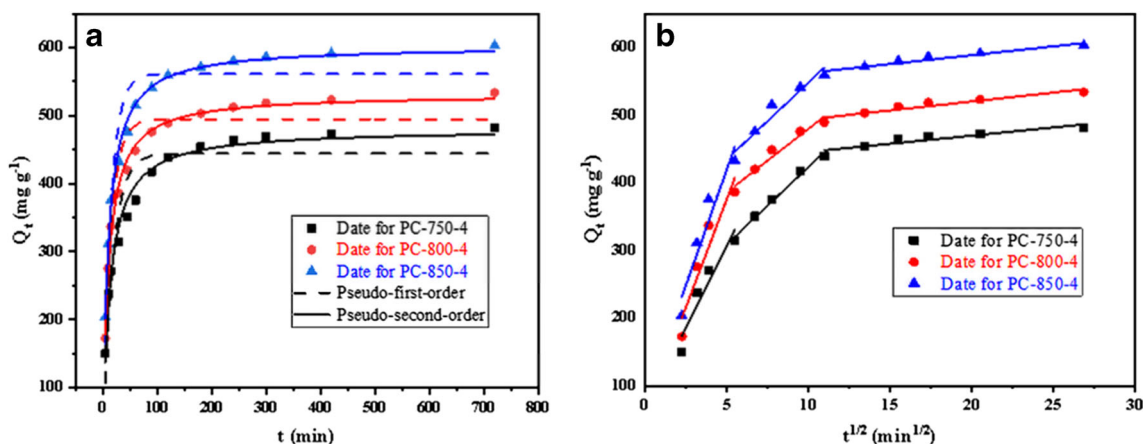


Fig. 8 The nonlinear fitting by **a** pseudo-first-order and pseudo-second-order rate model and **b** intra-particle diffusion model

amount of CAP adsorbed on PC-800-4 was as high as 263.8 mg L^{-1} . This implied that the humic acid molecules were not effectively absorbed by the pores inside PC-800-4, perhaps due to large molecular size of the acid. Based on the above results, we believe that PC-800-4 has a broad application prospect in the treatment of CAP-containing wastewater.

Adsorption isotherm analysis

The equilibrium adsorption isotherm model can be used to explain the adsorption mechanism of the adsorbent for the target. The Langmuir, Freundlich and Temkin isotherm models are suitable for single-layer physical adsorption on uniform surfaces, multi-layer adsorption on non-uniform surfaces, and strong electrostatic interactions between positive and negative charges. Figure 7 and Table 2 show the nonlinear fitting curves and parameters for PC-800-4 adsorption of CAP at different temperatures. It can be seen that the adsorption capacity of PC-800-4 was enhanced with the increasing temperature. The determination coefficient (R^2) values for the Langmuir, Freundlich, and Temkin models were in the

range of 0.9976–0.9992, 0.9786–0.9942, and 0.9650–0.9750, respectively. According to higher R^2 and the lower values of ARE, the correlation of isotherms was as follows: Langmuir > Freundlich > Temkin. Therefore, it can be deduced that the single-layer physical adsorption played a dominant role in the CAP adsorption by PC-800-4. At the same time, using the D-R isotherm equation to calculate $E = 7.514 < 8 \text{ kJ mol}^{-1}$, it was verified that physical adsorption was the dominant mechanism. The K_L value and K_F value increased with temperature, which may be related to the decrease in the inherent chemical properties of the adsorbent and the heterogeneity factor, respectively. In addition, the ratio $1/n$ can be used to judge the difficulty of adsorption. In the range of 298–308 K, $1/n$ was less than 0.5, indicating that PC easily adsorbed to CAP (Liang et al. 2020). Moreover, as the temperature increasing, the $1/n$ value gradually decreased, indicating that the temperature rise was conducive to increased adsorption. This was consistent with the chemical adsorption behavior. Therefore, it can be inferred that chemical adsorption played a role in promoting the removal of CAP by PC-800-4.

Table 3 Kinetic parameters for the adsorption of CAP onto PC-T-4 ($T = 750, 800, 850 \text{ }^\circ\text{C}$)

Model	Pseudo-first-order model					Pseudo-second-order model			
	$Q_{e, \text{exp}} (\text{mg g}^{-1})$	$Q_{e, \text{cal}} (\text{mg g}^{-1})$	$K_1 \times 10^{-2} (\text{min})^{-1}$	ARE (%)	R^2	$Q_{e, \text{cal}} (\text{mg g}^{-1})$	$K_2 \times 10^{-4} (\text{g mg}^{-1} \text{min}^{-1})$	ARE (%)	R^2
PC-750-4	481.5	444.14	5.5	10.32	0.8766	480.5	1.66	4.07	0.9786
PC-800-4	534	494.35	6.97	7.03	0.918	531.8	1.88	1.91	0.9931
PC-850-4	602.7	560.82	6.9	7.07	0.918	602.5	1.67	1.52	0.9942

Table 4 Intra-particle diffusion model parameters for the adsorption of CAP onto PC-T-4 ($T = 750, 800, 850\text{ }^{\circ}\text{C}$)

Model	Intra-particle diffusion								
	K_{p1} ($\text{mg g}^{-1} \text{min}^{1/2}$)	C	R^2	K_{p2} ($\text{mg g}^{-1} \text{min}^{1/2}$)	C	R^2	K_{p3} ($\text{mg g}^{-1} \text{min}^{1/2}$)	C	R^2
PC-750-4	48.41	65.04	0.8962	22.84	195.08	0.9889	2.42	421.34	0.8488
PC-800-4	57.59	63.77	0.9019	18.83	291.9	0.956	2.64	467.51	0.9023
PC-850-4	68.35	78.35	0.9134	22.69	321.5	0.9365	2.63	535.98	0.9305

Analysis of adsorption kinetics of PC-800-4

The adsorption rate is a key parameter that reflects the adsorption performance of the adsorbent. Computations based on different adsorption kinetic models can give better understanding of the performance and adsorption mechanism of the adsorbent. Figure 8 a shows the distribution of PC-T-4 ($T = 750, 800, 850\text{ }^{\circ}\text{C}$) adsorption profile overtime at 303 K and CAP concentration of 120 mg L^{-1} . The non-linear fitting results and dynamic parameters by pseudo-first-order and pseudo-second-order models are shown in Table 3. The fitting results show that the pseudo-second-order model can better describe the experimental data (higher R^2 and the lower values of ARE) than the pseudo-first-order model. It can be inferred that PC-T-4 had some chemical adsorption to CAP, and the mechanism may be attributed to its π - π EDA interaction (Sun et al. 2020).

The migration of the adsorbate from the solution to the surface of the adsorbent usually involves external diffusion, surface diffusion, and pore diffusion processes. For the intra-particle diffusion model, a multilinear graph means multiple rate-controlling steps. The fitting of the intra-particle diffusion with the coefficients is shown in Table 4. Figure 8 b shows that the adsorption process includes three diffusion steps: (1) CAP molecules rapidly diffuse from solution to the surface of PC-T-4; (2) CAP molecules diffuse into the interior of PC-T-4; and (3) an equilibrium is established.

Thermodynamic analysis of CAP adsorption

To investigate the effect of temperature on the adsorption of CAP, three temperatures of 298 K, 303 K, and 308 K were selected for thermodynamic experiments. As shown in Table 5, a positive value of ΔH indicates that the reaction is endothermic, which is consistent with the analysis described by kinetics and isotherms. A negative ΔG indicates that adsorption was a spontaneous process. As the temperature increased, the ΔG value gradually decreased from -6.2419 to $-6.9136\text{ kJ mol}^{-1}$, indicating that the adsorption reaction was favorable at high temperatures. In addition, the value of ΔG is in the range of -20 to 0 kJ mol^{-1} , indicating that the adsorption process was dominated by physical adsorption (Zhang et al. 2018), which is supported by the value of Langmuir isotherm R^2 . ΔS is an indicative measure of the system’s randomness. In this case, the value of ΔS indicates that the degree of system randomness increases after loading CAP molecules to PC-800-4.

Comparison with other adsorbents

The adsorption capacity is an important indicator for evaluating the performance of adsorbents. Table 6 compares the CAP removal capacity of this work and other developed adsorbents. It can be seen that the porous carbon prepared by this work still had a high adsorption capacity under the conditions of relatively low initial

Table 5 Thermodynamic parameters of CAP adsorption onto PC-800-4

C_0 (mg L^{-1})	Gibbs equation form	T (K)	ΔG (kJ mol^{-1})	ΔH (kJ mol^{-1})	ΔS (kJ mol^{-1})	R^2
120	$\Delta G = -RT \ln K_d$	298	-6.2419	13.79	0.067	0.9956
		303	-6.5389			
		308	-6.9136			

Table 6 Maximum CAP adsorption capacity of some adsorbents

Adsorbents	C_0 mg L ⁻¹	Adsorbent dosage mg L ⁻¹	Q_e mg g ⁻¹	Temperature K	Refs.
PCN-222	1000	1000	370	298	(Jin et al. 2020)
PNSBCop	600	1000	423.7	313	(Yang et al. 2020b)
HpZIF-8-10(1.5)	50	1000	16.4	298	(Chen et al. 2019)
MBC700	40	500	60.2	298	(Yang et al. 2020c)
ABA-16	400	1000	155.4	303	(Mohd Din et al. 2015)
PC-800-4	120	150	534	303	This work
PC-850-4	120	150	602.7	303	This work

concentration and dosage. Therefore, PC is a kind of adsorbent with great potential.

Conclusion

This work successfully transformed SLS into porous carbons through one-step activation method. It not only simplified the production process of porous carbon materials, but also realized the efficient adsorption of CAP, achieving the effect of treating wastes with wastes. At 303 K, the maximum adsorption capacity of the synthesized PC-800-4 at a lower initial concentration of CAP (120 mg L⁻¹) was 534.0 mg g⁻¹, which was a great improvement compared to the work of others. Analysis of the adsorption data showed that the Langmuir isotherm model and pseudo-second-order kinetics perfectly described the adsorption isotherm. Thermodynamic analysis of adsorption isotherm showed that the adsorption process of CAP was spontaneous and endothermic. An evaluation of the adsorption isotherm indicated that the physical and chemical synergistic effects favored the adsorption of CAP. It was exciting that the synthesized adsorbents maintained a high adsorption capacity in a complex water environment. PC-800-4 was considered to be a simple, low-cost, and efficient biomass-based porous carbon with broad application prospects.

Authors' contribution Conception and design of the research: Jiaju Pang and Xiao Wei. Acquisition of data: Aixia Chen, Bei Chen, Jiaju Pang, and Yaping Xie. Analysis and interpretation of the data: Jiaju Pang and Xiao Wei. Writing of the manuscript: Jiaju Pang and Aixia Chen. Critical revision of the manuscript for important intellectual content: Aixia Chen and Jiaju Pang. AC and JP contributed equally to this work.

Funding This work was supported by the National Postdoctoral Science Foundation (No. 2017M610618), Postdoctoral Science Foundation Funded Project of Shaanxi Province (No. 2017BSHEDZZ64), and Fundamental Research Funds for the Central Universities of Chang' an University (No. 300102290104).

Data availability The dataset used and/or analyzed during the current study are available from the corresponding author on reasonable request.

Compliance with ethical standards

Ethical approval and consent to participate Not applicable.

Consent to publish The authors confirm that the final version of the manuscript has been reviewed, approved, and consented for publication by all authors.

Competing interests The authors declare no competing interests.

References

- Abukhadra MR, Adlii A, Bakry BM (2019) Green fabrication of bentonite/chitosan@cobalt oxide composite (BE/CH@Co) of enhanced adsorption and advanced oxidation removal of Congo red dye and Cr (VI) from water. *Int J Biol Macromol* 126:402–413. <https://doi.org/10.1016/j.ijbiomac.2018.12.225>
- Awual MR (2016a) Assessing of lead(III) capturing from contaminated wastewater using ligand doped conjugate adsorbent. *Chem Eng J* 289:65–73. <https://doi.org/10.1016/j.cej.2015.12.078>
- Awual MR (2016b) Solid phase sensitive palladium(II) ions detection and recovery using ligand based efficient conjugate nanomaterials. *Chem Eng J* 300:264–272. <https://doi.org/10.1016/j.cej.2016.04.071>
- Awual MR (2017a) New type mesoporous conjugate material for selective optical copper(II) ions monitoring & removal from polluted waters. *Chem Eng J* 307:85–94. <https://doi.org/10.1016/j.cej.2016.07.110>
- Awual MR (2017b) Novel nanocomposite materials for efficient and selective mercury ions capturing from wastewater. *Chem Eng J* 307:456–465. <https://doi.org/10.1016/j.cej.2016.08.108>
- Awual MR (2019a) An efficient composite material for selective lead(II) monitoring and removal from wastewater. *J Environ Chem Eng* 7: 103087. <https://doi.org/10.1016/j.jece.2019.103087>
- Awual MR (2019b) Efficient phosphate removal from water for controlling eutrophication using novel composite adsorbent. *J Clean Prod* 228:1311–1319. <https://doi.org/10.1016/j.jclepro.2019.04.325>
- Awual MR, Hasan MM (2014) Novel conjugate adsorbent for visual detection and removal of toxic lead(II) ions from water. *Micropor Mesopor Mat* 196:261–269. <https://doi.org/10.1016/j.micromeso.2014.05.021>

- Awual MR, Hasan MM (2015) Fine-tuning mesoporous adsorbent for simultaneous ultra-trace palladium(II) detection, separation and recovery. *J Ind Eng Chem* 21:507–515. <https://doi.org/10.1016/j.jiec.2014.03.013>
- Bhatnagar A, Hogland W, Marques M, Sillanpää M (2013) An overview of the modification methods of activated carbon for its water treatment applications. *Chem Eng J* 219:499–511. <https://doi.org/10.1016/j.cej.2012.12.038>
- Carvalho IT, Santos L (2016) Antibiotics in the aquatic environments: a review of the European scenario. *Environ Int* 94:736–757. <https://doi.org/10.1016/j.envint.2016.06.025>
- Chen A, Xie Y, Wei X, Chen B, Pang J (2021) One-step preparation of sodium alginate-based porous carbon for the adsorption of Bisphenol A in water. *J Chem Eng Data*. <https://doi.org/10.1021/acs.jced.0c00894>
- Chen X, Jiang X, Yin C, Zhang B, Zhang Q (2019) Facile fabrication of hierarchical porous ZIF-8 for enhanced adsorption of antibiotics. *J Hazard Mater* 367:194–204. <https://doi.org/10.1016/j.jhazmat.2018.12.080>
- Cheng P, Gao S, Zang P, Yang X, Bai Y, Xu H, Liu Z, Lei Z (2015) Hierarchically porous carbon by activation of shiitake mushroom for capacitive energy storage. *Carbon* 93:315–324. <https://doi.org/10.1016/j.carbon.2015.05.056>
- Clesham K, Bhatnagar N, Samarasinghe S (2019) Diagnosis and management of childhood aplastic anaemia. *Paediatr Child Health* 29(8):327–333. <https://doi.org/10.1016/j.paed.2019.05.001>
- Dai J, Qin L, Zhang R, Xie A, Chang Z, Tian S, Li C, Yan Y (2018a) Sustainable bovine bone-derived hierarchically porous carbons with excellent adsorption of antibiotics: equilibrium, kinetic and thermodynamic investigation. *F Powder Technol* 331:162–170. <https://doi.org/10.1016/j.powtec.2018.03.005>
- Dai Y, Sun Q, Wang W, Lu L, Liu M, Li J, Yang S, Sun Y, Zhang K, Xu J, Zheng W, Hu Z, Yang Y, Gao Y, Chen X, Zhang X, Gao F, Zhang Y (2018b) Utilizations of agricultural waste as adsorbent for the removal of contaminants: a review. *Chemosphere* 211:235–253. <https://doi.org/10.1016/j.chemosphere.2018.06.179>
- Dissanayake Herath GA, Poh LS, Ng WJ (2019) Statistical optimization of glyphosate adsorption by biochar and activated carbon with response surface methodology. *Chemosphere* 227:533–540. <https://doi.org/10.1016/j.chemosphere.2019.04.078>
- Galkin MV, Samec JSM (2016) Lignin valorization through catalytic lignocellulose fractionation: a fundamental platform for the future biorefinery. *ChemSusChem* 9(13):1544–1558. <https://doi.org/10.1002/cssc.201600237>
- Gao Y, Yue Q, Gao B, Sun Y, Wang W, Li Q, Wang Y (2013) Preparation of high surface area-activated carbon from lignin of papermaking black liquor by KOH activation for Ni(II) adsorption. *Chem Eng J* 217:345–353. <https://doi.org/10.1016/j.cej.2012.09.038>
- George AM, Hall RM (2002) Efflux of chloramphenicol by the CmlA1 protein. *FEMS Microbiol Lett* 209(2):209–213. [https://doi.org/10.1016/S0378-1097\(02\)00558-X](https://doi.org/10.1016/S0378-1097(02)00558-X)
- Jimenez JJ, Jimenez JG, Daghistani D, Yunis AA (1990) Interaction of chloramphenicol and metabolites with colony stimulating factors: possible role in chloramphenicol-induced bone marrow injury. *Am J Med Sci* 300(6):350–353. <https://doi.org/10.1097/00000441-199012000-00002>
- Jin E, Lee S, Kang E, Kim Y, Choe W (2020) Metal-organic frameworks as advanced adsorbents for pharmaceutical and personal care products. *Coord Chem Rev* 425:213526. <https://doi.org/10.1016/j.ccr.2020.213526>
- Kikuchi H, Sakai T, Teshima R, Nemoto S, Akiyama H (2017) Total determination of chloramphenicol residues in foods by liquid chromatography-tandem mass spectrometry. *Food Chem* 230:589–593. <https://doi.org/10.1016/j.foodchem.2017.03.071>
- Li M, Liu Y, Zeng G, Liu N, Liu S (2019) Graphene and graphene-based nanocomposites used for antibiotics removal in water treatment: a review. *Chemosphere* 226:360–380. <https://doi.org/10.1016/j.chemosphere.2019.03.117>
- Liang H, Sun R, Song B, Sun Q, Peng P, She D (2020) Preparation of nitrogen-doped porous carbon material by a hydrothermal-activation two-step method and its high-efficiency adsorption of Cr(VI). *J Hazard Mater* 387:121987. <https://doi.org/10.1016/j.jhazmat.2019.121987>
- Liu J, Zhou D, Xu Z, Zheng S (2017b) Adsorptive removal of pharmaceutical antibiotics from aqueous solution by porous covalent triazine frameworks. *Environ Pollut* 226:379–384. <https://doi.org/10.1016/j.envpol.2017.03.063>
- Liu WJ, Jiang H, Yu HQ (2015) Thermochemical conversion of lignin to functional materials: a review and future directions. *Green Chem* 17(11):4888–4907. <https://doi.org/10.1039/C5GC01054C>
- Liu X, Steele JC, Meng X (2017a) Usage, residue, and human health risk of antibiotics in Chinese aquaculture: a review. *Environ Pollut* 223:161–169. <https://doi.org/10.1016/j.envpol.2017.01.003>
- Liu Z, Adewuyi YG, Shi S, Chen H, Li Y, Liu D, Liu Y (2019) Removal of gaseous Hg0 using novel seaweed biomass-based activated carbon. *Chem Eng J* 366:41–49. <https://doi.org/10.1016/j.cej.2019.02.025>
- Lü G, Wu L, Wang X, Liao L, Wang X (2012) Adsorption of chlortetracycline from water by rectories. *Chinese J Chem Eng* 20(5):1003–1007. [https://doi.org/10.1016/S1004-9541\(12\)60429-7](https://doi.org/10.1016/S1004-9541(12)60429-7)
- Lu J, Sun J, Chen X, Tian S, Chen D, He C, Xiong Y (2019) Efficient mineralization of aqueous antibiotics by simultaneous catalytic ozonation and photocatalysis using MgMnO₃ as a bifunctional catalyst. *Chem Eng J* 358:48–57. <https://doi.org/10.1016/j.cej.2018.08.198>
- Mauer SM, Chavers BM, Kjellstrand CM (1980) Treatment of an infant with severe chloramphenicol intoxication using charcoal-column hemoperfusion. *J Pediatr* 96(1):136–139. [https://doi.org/10.1016/S0022-3476\(80\)80350-7](https://doi.org/10.1016/S0022-3476(80)80350-7)
- Lv K, Han J, Yang C, Cheng C, Luo Y, Wang X (2016) A category of hierarchically porous tin (IV) phosphonate backbone with the implication for radioanalytical separation. *Chem Eng J* 302:368–376. <https://doi.org/10.1016/j.cej.2016.05.061>
- Mohd Din AT, Ahmad MA, Hameed BH (2015) Ordered mesoporous carbons originated from non-edible polyethylene glycol 400 (PEG-400) for chloramphenicol antibiotic recovery from liquid phase. *Chem Eng J* 260:730–739. <https://doi.org/10.1016/j.cej.2014.09.010>
- Oginni O, Singh K, Oporto G, Dawson-Andoh B, McDonald L, Sabolsky E (2019) Influence of one-step and two-step KOH activation on activated carbon characteristics. *Bioresource Technology Reports* 7:100266. <https://doi.org/10.1016/j.biteb.2019.100266>
- Sarkar A, Paul B (2020) Analysis of the performance of zirconia-multiwalled carbon nanotube nanoheterostructures in adsorbing As(V) from potable water from the aspects of physical chemistry with an emphasis on adsorption site energy distribution and density functional theory calculations. *Micropor Mesopor Mat* 302:110191. <https://doi.org/10.1016/j.micromeso.2020.110191>
- Saygılı H, Saygılı GA (2019) Optimized preparation for bimodal porous carbon from lentil processing waste by microwave-assisted K₂CO₃ activation: spectroscopic characterization and dye decolorization activity. *J Clean Prod* 226:968–976. <https://doi.org/10.1016/j.jclepro.2019.04.121>
- Srinivasa Raghavan DS, Qiu G, Ting Y (2018) Fate and removal of selected antibiotics in an osmotic membrane bioreactor. *Chem Eng J* 334:198–205. <https://doi.org/10.1016/j.cej.2017.10.026>
- Sun S, Jiao C, Xu Z, Yang Z, Peng S (2020) KOH activated ZIF-L derived N-doped porous carbon with enhanced adsorption performance towards antibiotics removal from aqueous solution. *J Solid State Chem* 289:121492. <https://doi.org/10.1016/j.jssc.2020.121492>

- Tian S, Dai J, Jiang Y, Chang Z, Xie A, He J, Zhang R, Yan Y (2017) Facile preparation of intercrossed-stacked porous carbon originated from potassium citrate and their highly effective adsorption performance for chloramphenicol. *J Colloid Interf Sci* 505:858–869. <https://doi.org/10.1016/j.jcis.2017.06.062>
- Wang T, Wei X, Zong Y, Zhang S, Guan W (2020) An efficient and stable fluorescent sensor based on APTES-functionalized CsPbBr₃ perovskite quantum dots for ultrasensitive tetracycline detection in ethanol. *J Mater Chem C* 35:12196–12203. <https://doi.org/10.1039/D0TC02852E>
- Wei C, Li X, Xie Y, Wang X (2019) Direct photo transformation of tetracycline and sulfanamide group antibiotics in surface water: kinetics, toxicity and site modeling. *Sci Total Environ* 686:1–9. <https://doi.org/10.1016/j.scitotenv.2019.04.041>
- Wu Z, Huang W, Shan X, Li Z (2020) Preparation of a porous graphene oxide/alkali lignin aerogel composite and its adsorption properties for methylene blue. *Int J Biol Macromol* 143:325–333. <https://doi.org/10.1016/j.ijbiomac.2019.12.017>
- Xie A, Cui J, Chen Y, Lang J, Li C, Yan Y, Dai J (2019a) Simultaneous activation and magnetization toward facile preparation of auricularia-based magnetic porous carbon for efficient removal of tetracycline. *J Alloy Compd* 784:76–87. <https://doi.org/10.1016/j.jallcom.2018.12.375>
- Xie A, Dai J, Chen Y, Liu N, Ge W, Ma P, Zhang R, Zhou Z, Tian S, Li C, Yan Y (2019b) NaCl-template assisted preparation of porous carbon nanosheets started from lignin for efficient removal of tetracycline. *Adv Powder Technol* 30(1):170–179. <https://doi.org/10.1016/j.apt.2018.10.020>
- Yang F, Zhang Q, Jian H, Wang C, Xing B, Sun H, Hao Y (2020c) Effect of biochar-derived dissolved organic matter on adsorption of sulfamethoxazole and chloramphenicol. *J Hazard Mater* 396:122598. <https://doi.org/10.1016/j.jhazmat.2020.122598>
- Yang J, Dai J, Wang L, Ge W, Xie A, He J, Yan Y (2019) Ultrahigh adsorption of tetracycline on willow branch-derived porous carbons with tunable pore structure: isotherm, kinetics, thermodynamic and new mechanism study. *J Taiwan Inst Chem E* 96:473–482. <https://doi.org/10.1016/j.jtice.2018.12.017>
- Yang J, Ji G, Gao Y, Fu W, Irfan M, Mu L, Zhang Y, Li A (2020b) High-yield and high-performance porous biochar produced from pyrolysis of peanut shell with low-dose ammonium polyphosphate for chloramphenicol adsorption. *J Clean Prod* 264:121516. <https://doi.org/10.1016/j.jclepro.2020.121516>
- Yang V, Arumugam Senthil R, Pan J, Rajesh Kumar T, Sun Y, Liu X (2020a) Hierarchical porous carbon derived from jujube fruits as sustainable and ultrahigh capacitance material for advanced supercapacitors. *J Colloid Interf Sci* 579:347–356. <https://doi.org/10.1016/j.jcis.2020.06.080>
- Ye Q, Xu H, Zhang J, Wang Q, Zhou P, Wang Y, Lu J (2020) Enhancement of peroxymonosulfate activation for antibiotics removal by nano zero valent tungsten induced Cu(II)/Cu(I) redox cycles. *Chem Eng J* 382:123054. <https://doi.org/10.1016/j.cej.2019.123054>
- Zhang L, Song X, Liu X, Yang L, Pan F, Lv J (2011) Studies on the removal of tetracycline by multi-walled carbon nanotubes. *Chem Eng J* 178:26–33. <https://doi.org/10.1016/j.cej.2011.09.127>
- Zhang W, Chen J, Hu Y, Fang Z, Cheng J, Chen Y (2018) Adsorption characteristics of tetrabromobisphenol A onto sodium bisulfite reduced graphene oxide aerogels. *Colloids Surf A Physicochem Eng Asp* 538:781–788. <https://doi.org/10.1016/j.colsurfa.2017.11.070>
- Zhang X, Li Y, Hou Y (2019) Preparation of magnetic polyethylenimine lignin and its adsorption of Pb(II). *Int J Biol Macromol* 141:1102–1110. <https://doi.org/10.1016/j.ijbiomac.2019.09.061>
- Zhou Y, Zhang L, Cheng Z (2015) Removal of organic pollutants from aqueous solution using agricultural wastes: a review. *J Mol Liq* 212:739–762. <https://doi.org/10.1016/j.molliq.2015.10.023>

Publisher's note Springer Nature remains neutral with regard to jurisdictional claims in published maps and institutional affiliations.